Frequency Analysis of Microcluster Halftoning

Henry R. Kang
Xerox Corporation, SDSP/ODPG
Mail Stop 820-03F, 200 Crosskey Office Park, Fairport, NY. 14450

Abstract

Microcluster halftoning is a hybrid approach between clustered-dot and dispersed-dot ordered dithers. The goals of the microcluster halftoning are to overcome the tradeoff between screen frequency and tone level of clustered dots, to minimize distinctive structures of dispersed dots, and to reduce the graininess. Basically, the microcluster halftoning is an integration of the frequency modulation, super cell, multi-center dot, and nucleus randomization. First, a halftone cell is divided into small subcells. A general cell partition technique is used for dividing halftone cells. The frequency modulation is employed to disperse the nuclei among subcells. A general pixel dispersion scheme is developed for this purpose. In addition, a stochastic nucleus randomization within the subcell is possible to provide a more homogeneous nucleus dispersion. Once the nuclei are established, the classical clustered-dot order dither is used for further dot growth. A series of dots based on these principles is designed and the frequency spectra are computed by using the Fourier transform. Results are compared to the clustered-dot and dispersed-dot approaches.

Introduction

A major problem in clustered-dot ordered-dither halftoning is the conflicting requirements for high screen frequency and high tone level.[1] This is because the frequency is inversely proportional to the square root of the tone level. If one increases the frequency for the purpose of obtaining finer details and making the screen less visible, the tone level will be decreased. This raises the chance of false contouring. On the other hand, if one increases the tone level, thereby decreasing the likelihood of contours, the cell size becomes larger and the screen becomes coarser and more visible. The finer details will be lost. The problem of frequency-level tradeoff can be eliminated by using the dispersed-dot ordered dither, frequency modulation (FM), or stochastic screening. Unlike clustered-dot, these methods do not have the constraints of the screen frequency and angle. Pixels in a dispersed-dot are ordered in such a way that the total "on" positions in the array[3] at any instance of ordering are distributed as homogeneously as possible. Although these dispersed-dot patterns are homogeneous, they suffer from rigid regular structures. This problem is reduced by the random nucleated screens to break up the regularity, and the developments of blue-noise mask (BNM) and void-and-cluster methods.[2-7] These developments lead to the ever-popular stochastic screening. Many advantages have been claimed, such as no visible dot pattern, no morie, no tradeoff between tone level and frequency, and no tone jump. It, however, shows graininess or noisy appearance, has severe dot gain problems across the whole tone range, and requires a stable, reproducible printer. In addition to these problems, there are penalties to the cost and speed. For example, to properly disperse pixels for minimizing textures requires large screen size, thus more memory to store it. For screenless halftoning such as error diffusion, the computation cost is usually high. Moreover, it is difficult to fine tune a large screen and it is not possible to fine tune screenless approaches. These problems make color proofing more difficult.

In this paper, we present a new microcluster approach that can reduce the problems of the stochastic screening. Microcluster halftoning is a hybrid approach between clustered-dot and dispersed-dot ordered dithers. The goals of the microcluster halftoning are to overcome the tradeoff between screen frequency and tone level of clustered dots, to minimize distinctive structures of dispersed dots in the highlight region, and to reduce the graininess. The concept and design principles of microcluster dots have been presented by Kang in 1995.[8] Basically, the microcluster halftoning is an integration of the frequency modulation, super cell, multi-center dot, and nucleus randomization.[2,3,9,10] First, a halftone cell is divided into small subcells. A general cell partition technique is used for dividing halftone cells. Then, positions of nuclei for subcells are established by using frequency modulation. A general pixel dispersion scheme is developed to disperse the nuclei among subcells. Because a subcell contains multiple pixels, it is possible to stochastically randomized nucleus within the subcell for the purpose of providing a more homogeneous nucleus dispersion among subcells. Once the nuclei are established, the classical clustered-dot order dither is used for further dot growth. A series of dots based on these principles is designed and the frequency spectra are computed by using the Fourier transform. Results are compared to the clustered-dot and dispersed-dot approaches.

Fourier Transform

Fourier transform has been used to solve a large number of linear problems ranging from mechanical engineering to economy. It is the foundation of the linear signal filtering in electronic imaging. In printing, it has been used to derive the optimal dispersed-dot screens, to study classical halftone screens, to examine image induced artifacts due to interaction with clustered and dispersed-dot ordered dither on square grids, and to compute and display the Fourier spectrum of ordered dither in terms of the continuous-space dimensions of rectangular and hexagonal grids.[11-15] This analysis follows the method developed by Ulichney.[14,15]

The binary output from halftoning a gray level input by means of ordered dither is periodic with the same spatial period as the threshold array. The spatial period is specified by two vectors, p_x and p_y , in terms of the spatial sampling vectors, v_x and v_y

$$p_x = Nv_x \text{ and } p_y = Nv_y,$$

for some integer N. The sampling vectors can be thought of as grid generating vectors. The Discrete Fourier Transform (DFT) of an even period is

$$C(\mathbf{f}) = (|\det \mathbf{P}|)_{-1} \sum I[\mathbf{k}]\, \delta\, (\mathbf{f} - \mathbf{Q}\, \mathbf{k}) , \qquad (1)$$

where, in scalar notation,

$$I[\mathbf{k}] = I[k_1, k_2] = \sum\sum I[n_1, n_2] \exp\{-j2\pi\, (k_1n_1+k_2n_2)/N\} \quad (2)$$

is the two-dimensional DFT. This equation applies to periodic grids in general. For the case of rectangular grids, the matrices involved can be expressed in terms of the sample and line periods:

$$V = \begin{bmatrix} S & 0 \\ 0 & L \end{bmatrix}, \quad U = \begin{bmatrix} S^{-1} & 0 \\ 0 & L^{-1} \end{bmatrix},$$

$$P = \begin{bmatrix} NS & 0 \\ O & NL \end{bmatrix}, \quad Q = \begin{bmatrix} (NS)^{-1} & 0 \\ 0 & (NL)^{-1} \end{bmatrix},$$

$$\text{and } f^T = k^T Q^T,$$

where superscript T represents the transpose of a matrix or vector that is obtained by exchanging lines with correspon-ding columns. One limitation of this equation is that it is only valid for periods which have a perfect square number of elements. For non-square periods (or threshold arrays), Ulichney utilizes the Similarity Theorem that the transform of k periods as one period results a scaled DFT; each nonzero frequency component in the resulting DFT is accompanied by k zero coefficients and have a magnitude k times as large as the DFT of a single period.[16] Therefore, packing odd tiles in this way only requires the additional step of dividing the resulting DFT by k.

The magnitude spectrum of DFT provides insights into the relative distribution of energy in frequency domain. In this application, a composite DFT which summarizes the energy distributions over all tone levels for a given threshold array is used. This composite DFT is defined as the sum of absolute DFT values at every possible tone level, then the result is divided by the total number of tone levels:

$$I_{sum}[k] = (Z+1)_{-1} \sum |[k; g]| \qquad (3)$$

where Z is the total number of tone levels excluding the zero tone level. Substituting Eq. (3) into Eq. (1) yields a specification of the location and magnitude of Fourier transform impulses. The computed $\mathbf{I}_{sum}$ [**k**] can be displayed with dots of an area proportional to the magnitude of the impulse. Such a display is similar to a photograph of an optical Fourier transform consisting of points of light with different intensity; the resulting size of exposed points would be proportional to their magnitude. Based on this similarity, Ulichney named them "exposure plots" .

Fourier Analyses of Clustered Dots

Based on the conventional practice of color printing, the black screen is set at 45º. Cyan and magenta screens are rotated 30º away from the black, having values 15º and 75º, respectively. The lightest color, yellow, is placed at 0º (or 90º). In this study, the clustered-dots are used as the baseline information for comparisons with microcluster dots. These clustered-dots are rational tangent screens that the screen angles must be a tangent of integer ratio. Because of this constraint, the exact 15º (or 75º) angle is not achievable at the tone levels employed in this study. Moreover, the differences in screen angles lead to slightly different screen frequencies and tone levels for four primary colors with the exception that cyan screen is the mirror image of the magenta screen. The first set of screens is small dots with tone levels of 10, 10, 9, and 8 (these numbers are Z values which do not include the white level of no "on" pixel) for cyan, magenta, yellow, and black, respectively. Their threshold arrays are given in Figure 1; they are clustered-dots in a spiral pattern with screen angles of 18º, 72º, 0º, and 45º, for cyan, magenta, yellow, and black, respectively. For cyan and magenta screens, the resulting angles are the closest approximations to 15º and 75º at this dot size (10 pixels) by the rational tangent screen.

Cyan	Magenta	Yellow	Black
5 7	7 5		5
4 1 10	10 1 4	5 6 8	6 1 4
8 3 2 6	6 2 3 8	7 1 4	2 3 8
9	9	9 2 3	7

Figure 1. The threshold arrays of small clustered-dots.

The black at 45º can be coded into a rectangular block by using the Holladay algorithm.[17] The resulting block has the width (in pixels) exactly twice of the height. It takes two 45º screens to make a square, indicating an odd period. This is evidenced in the exposure plot of Figure 2a; a

characteristic diagonal orientation of the energy distribution in the frequency domain. The highest energy other than the zero frequency locates in the midway between the center and corners of baseband, showing the low frequency characteristic of a clustered dot. But, substantial energy distributes at corners, 1/(2S) cycles/unit-length where the highest possible frequencies reside, indicating the relative high frequency characteristic of a small dot.

The yellow screen at 0° is a square array with 3 × 3 elements. This is an even period threshold array with an odd number of elements on each side. It poses an interesting problem that the frequency sample at 1/(2S) is not an integer. To correct this problem, we employ the Similarity Theorem by packing four 3 × 3 screens into a 6×6 cell. The resulting exposure plot for yellow screen is given in Figure 2b; the horizontal and vertical periods are 3 units, there exists no energy at the edges of the baseband. Instead, the highest energy distributions are located at 1/(3S), showing the high frequency characteristic of a small dot.

Because of their size and shape, the Fourier analysis of cyan or magenta screen requires the packing of ten screens to give a 10 × 10 square cell in order to use the Similarity Theorem. Resulting exposure plots are depicted in Figs. 2c and 2d. The shape of the baseband is still square, but the energy distribution is no longer uniform. The magenta screen orients more toward horizontal direction and cyan orients more toward vertical direction, indicating the angular orientation of the screen.

Utilizing the linear property of the Fourier transform, we obtain the combined effort from individual screens.[18]

$$F\{h_c(x,y)\, I_c(x,y) + h_m(x,y)\, I_m(x,y) + h_y(x,y)\, I_y(x,y) + h_k(x,y)\, I_k(x,y)\}$$

$$= F\{h_c(x,y)\, I_c(x,y)\} + F\{h_m(x,y)\, I_m(x,y)\}$$

$$+ F\{h_y(x,y)\, I_y(x,y)\} + F\{h_k(x,y)\, I_k(x,y)\},$$

where F is the Fourier transform operator, I_c, I_m, I_y, and I_k are cyan, magenta, yellow, and black separations of the image, and h_c, h_m, h_y, and h_k are their corresponding halftone threshold arrays. To see the combined effort of threshold arrays on any arbitrary image, we need only analyze the threshold arrays themselves

$$F\{h_c(x,y) + h_m(x,y) + h_y(x,y) + h_k(x,y)\}$$

$$= F\{h_c(x,y)\} + F\{h_m(x,y)\} + F\{h_y(x,y)\} + F\{h_k(x,y)\}.$$

Figure 2e gives the combined spectrum of all four screens by summing them together. It shows that high energy sites from four primary colors form a ring surrounding the zero-frequency center with a radius about 1/(3S). Very little energy is located inside this ring, showing a relatively high frequency characteristic of small dots. The center and four corners are drawn as a four-concentric circle to indicate that they are overlapped four times; the number of circles in the concentric circle represents the number of overlaps.

The second set of primary screens has 17, 17, 16, and 18 tone levels for cyan, magenta, yellow, and black, respectively. Figure 3 gives the threshold arrays.

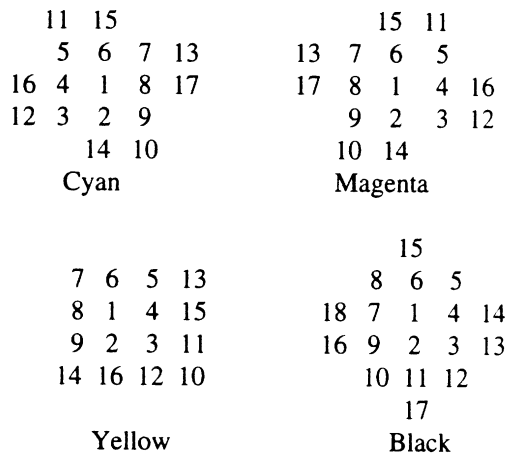

Figure 3. The threshold arrays of the second set of screens

The exposure plot of the black screen is given in Figure 4a, its energy distribution concentrates around the center in an odd fashion. The yellow threshold array is a perfect 4 × 4 square, giving an even and rectangular energy distribution. A majority of the energy is distributed in the low frequency (≤1/[4S]) region as shown in Figure 4b. For magenta and cyan and dots, 17 screens are packed together to give a square 17 × 17 cells. Once again, the Fourier spectra shown in Figs. 4c and 4d are not uniform, indicating an angular orientation. The combined Fourier spectrum is depicted in Figure 4e, several rings are formed by these screens. The highest energy sites form the closest ring with a radius about 1/(4S), the energy gradually reduces as the frequency increases. This spectrum clearly shows that the larger dots (as compared to the first set of screens) have more low frequency components.

The third set of screens has 40, 40, 36, and 32 tones for cyan, magenta, yellow, and black, respectively. Figure 5 gives the threshold arrays of this set of screens. They are exactly four times larger than the first set. The exposure plots of Figure 6 indicate that, as the number of tone level increases, the additional frequency terms in the Fourier transform assume positions between those of smaller dots with proportionally less energy in them. The size of the baseband, however, remains the same. The combined Fourier spectrum is given in Figure 6e.

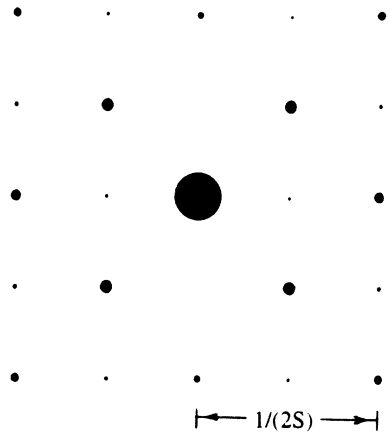

Fig. 2a. Black screen of 45 degrees.

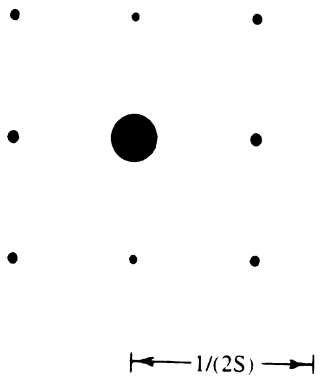

Fig. 2b. Yellow screen of 0 degree.

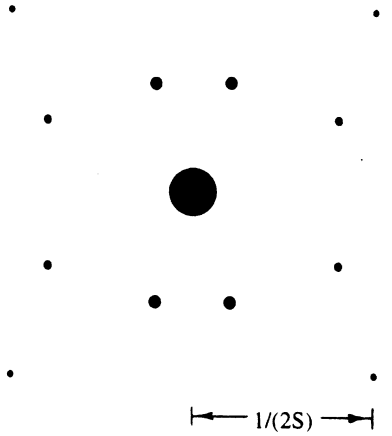

Fig. 2c. Magenta screen of 72 degrees.

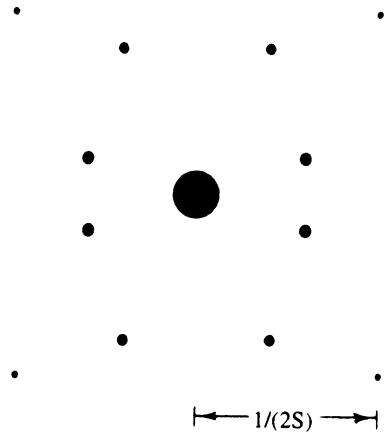

Fig. 2d. Cyan screen of 18 degrees.

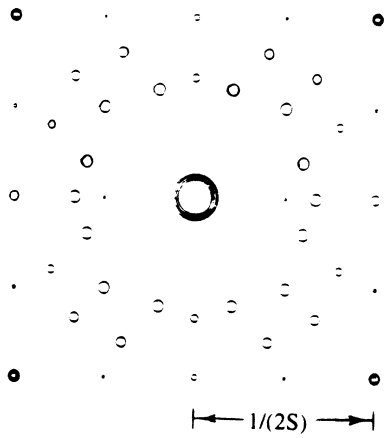

Fig. 2e. The sum of all four spectra.

Figure 2. Fourier exposure plots of small dots with tone levels of 10, l0, 9, and 8 levels for cyan, magenta, yellow and black, respectively, and the sum of all four spectra.

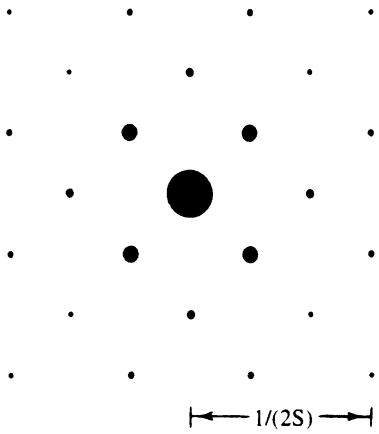

Fig. 4a. Black screen of 45 degrees.

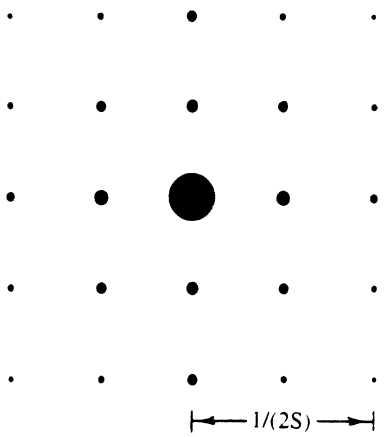

Fig. 4b. Yellow screen of 0 degree.

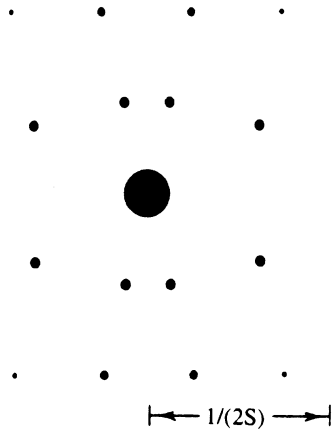

Fig. 4c. Magenta screen of 76 degrees.

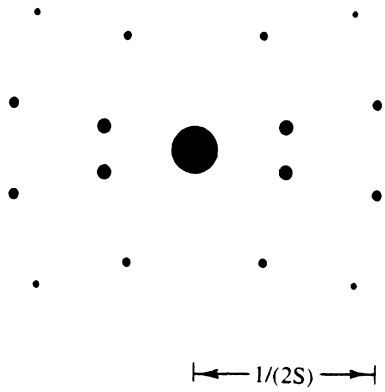

Fig. 4d. Cyan screen of 14 degrees.

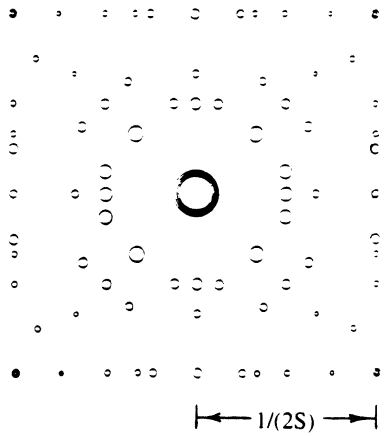

Fig. 4e. The sum of all four spectra.

Figure 4. Fourier exposure plots of small dots with tone levels of 17, 17, 16, and 18 levels for cyan, magenta, yellow and black, respectively, and the sum of all four spectra.

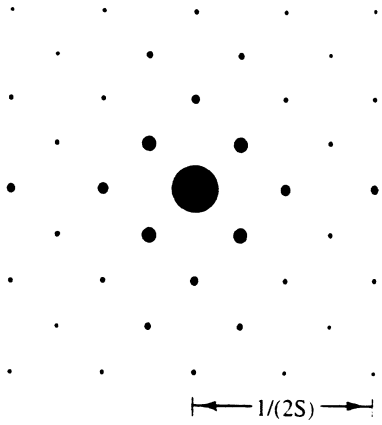

Fig. 6a. Black screen of 45 degrees.

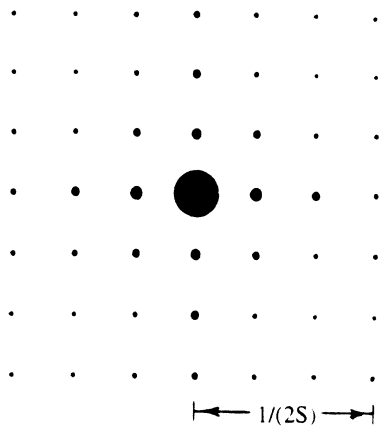

Fig. 6b. Yellow screen of 0 degree.

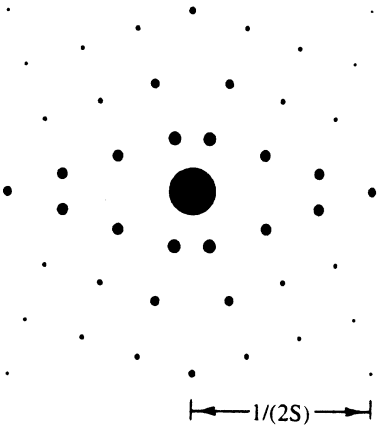

Fig. 6c. Magenta screen of 72 degrees.

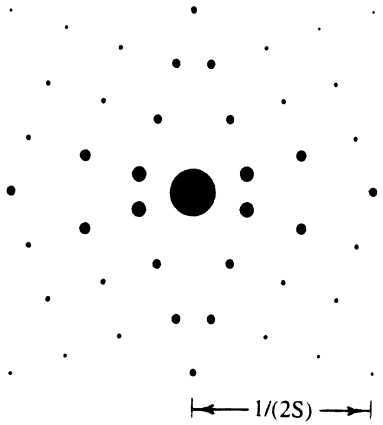

Fig. 6d. Cyan screen of 18 degrees.

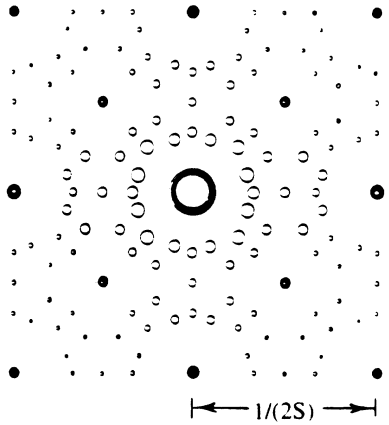

Fig. 6e. The sum of all four spectra.

Figure 6. Fourier exposure plots of small dots with tone levels of 40, 40, 36, and 32 levels for cyan, magenta, yellow and black, respectively, and the sum of all four spectra.

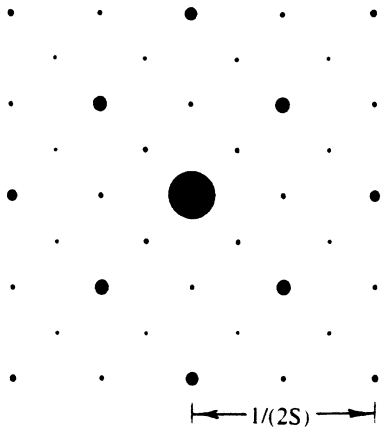

Fig. 8a. Black screen of 45 degrees.

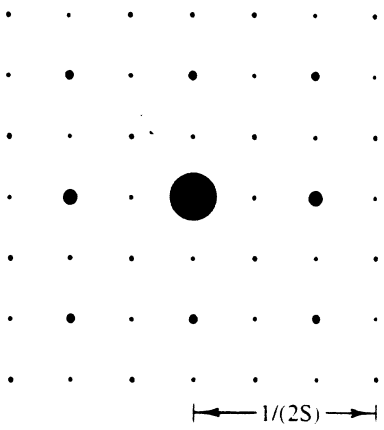

Fig. 8b. Yellow screen of 0 degree.

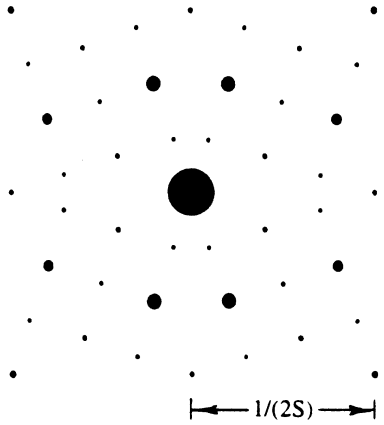

Fig. 8c. Magenta screen of 72 degrees.

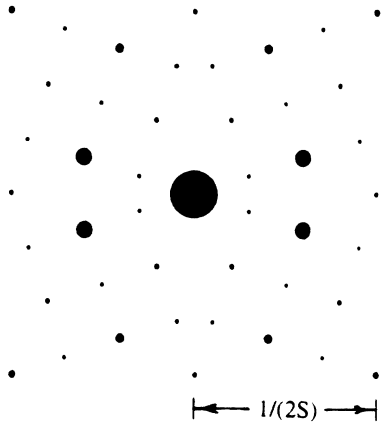

Fig. 8d. Cyan screen of 18 degrees.

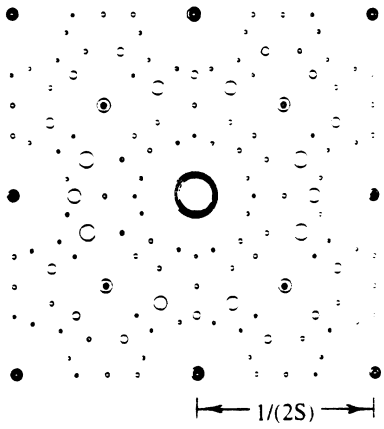

Fig. 8e. The sum of all four spectra.

Figure 8. Fourier exposure plots of small dots with tone levels of 40, 40, 36, and 32 levels for cyan, magenta, yellow and black, respectively, and the sum of all four spectra.

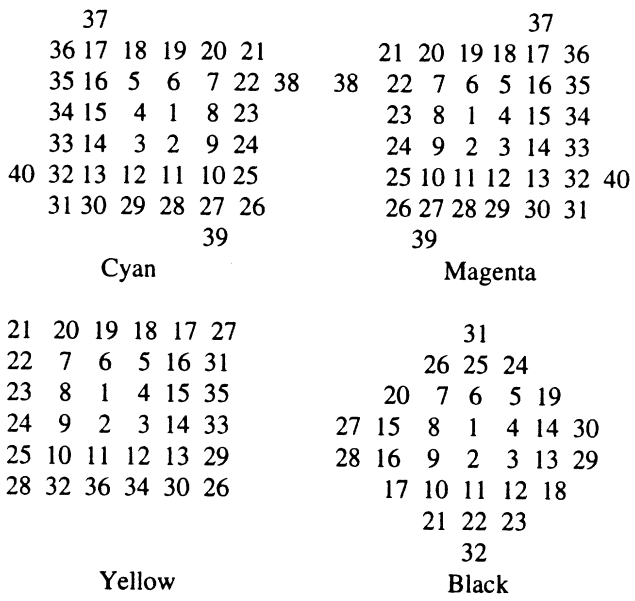

Figure 5. Threshold arrays of the third set of clustered dots.

Fourier Analyses of Quad-Dots

The third set of screens, having sufficient number of pixels, makes them eligible to be divided into smaller components such as four subcells (quad-dot). Figure 7 shows the threshold arrays of these quad-dots; each screen is divided into four equal sections. Because of the interception between the digital grid and the halftone cell boundary, the size and shape of subcells represented by digitized pixels may not be the same (see Figure 7). The exposure plots of Figure 8 look like the plots in Figure 2, especially the locations of high energy sites are identical. The difference is that the exposure plots of Figure 8 have many low energy sites populated in the high frequency region (>1/[4S]) as well as a few in the low frequency region (<1/[4S]). This introduces some low frequency components in the tone ramps. However, they don't seem to degrade the image quality because of the low population. Compared to the corresponding clustered-dot spectra of Figure 6, the high energy sites are moved away from the zero-frequency center, showing some dispersed nature. The combined spectrum of four screens is plotted in Figure 8e. Again, the spectrum is very similar to the first set (see Figure 4e).

Fourier Analyses of Microcluster Dots

The advantages of microcluster dots are illustrated by using a set of dots with 130, 130, 144, and 128 levels for cyan, magenta, yellow, and black, respectively. This set of screens gives screen angles of 15.255° , 74.745°, 0°, and 45°, respectively. The first advantage is that it provides better approximations to the 15° and 75° angles. Threshold arrays of the initial clustered-dots are given in Figure 9. The Fourier spectrum of the 45°, 128-level clustered-dot is given in Figure 10a and the spectrum of 0°, 144-level is given in Figure 11a.

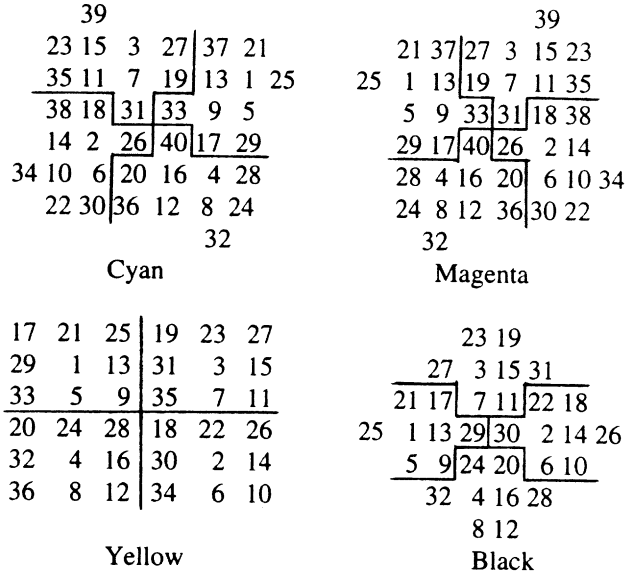

Figure 7 Threshold arrays of quad-dots.

This set of screens is successively divided into smaller components ranging from 2 to 16 subcells. Figure 12 shows the threshold arrays of dual-dots. The screen pattern is grown in a way that it has two hills and two valleys in opposite corners. The advantage of this dot pattern is to achieve the condition that the white areas on color when the area coverage is greater than 50% are the inverse images of colored dots on white when the area coverage is less than 50%.[1] Fourier spectra of the black and yellow dual-dots are shown in Figure 10b and Figure 11b, respectively. As soon as the screen is subdivided, the odd energy sites in both horizontal and vertical directions drop to a very small value and the high energy distributions move away from the zero frequency center. Similar behaviors are shown in cyan and magenta screens. Figure 13 gives the threshold arrays of quad-dots. Fourier spectra of the black and yellow quad-dots are shown in Figure 10c and Figure 11c, respectively; positions of high energy distributions are moving farther away from the center. The next set is divided into 8 parts; its threshold arrays are shown in Figure 14. Fourier spectra of the black and yellow screens are depicted in Figure 10d and Figure 11d, respectively. The last set of screens is divided into 16 subcells. Threshold arrays of the last microcluster dots are given in Figure 15, and the Fourier spectra of the black and yellow screens are shown in Figure 10e and Figure 11e, respectively. It is apparent that more energy is distributed farther away from the center as the partition becomes finer. For comparisons, the completely dispersed black screen is given in Figure 10f; the highest energy distributions are located at the corners of the baseband. This is different from the microcluster dot of Figure 10e that the energy is about equal at two frequency locations of 1/(4S) and 1/(2S). This is the purpose of the microcluster halftoning to retain some low frequency components in the midtone region.

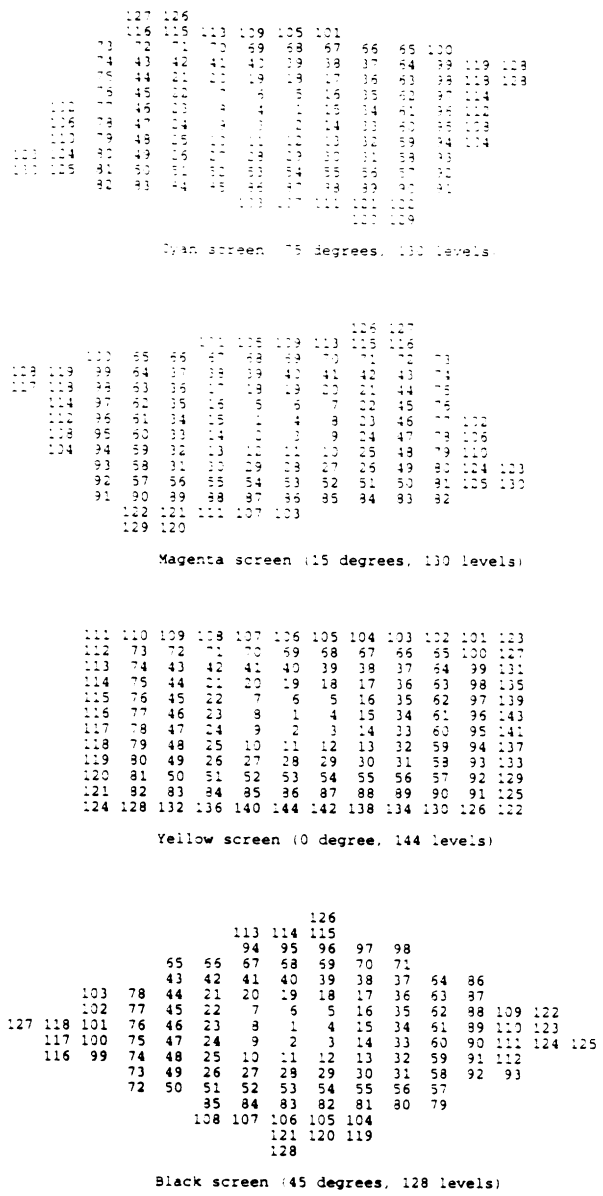

Figure 9. Threshold arrays of initial clustered-dots.

Experimental Results

The gray scale and color ramps of all screens are printed by using a HP Color LaserJet printer. They are arranged in 64 square patches, each patch has constant CMYK values. The gray and constant color ramps are chosen to display the halftone texture because, as pointed out by Ulichney, the most characteristic feature of a halftone technique is the texture generated in areas of uniform colors.[15] Thus, the best measure of the virtues of a halftone algorithm is its ability to render areas of uniform grays and constant colors. Using the textures of small clustered-dots as the standard for comparison, we find that the textures of microcluster quad-dots look like somewhere between the third set (with 40, 40, 36, and 32 levels) and the second set (with 17, 17, 16, and 18 levels) of clustered-dots. The microcluster octa-dots look like somewhere between the second and first sets. The microcluster hexdeca-dots show finer textures than the first set of clustered-dots.

Conclusion

Microcluster dots blend the characteristics of dispersed-dot and clustered-dot. Generally, they behave like a dispersed dot in the highlight region, a high frequency clustered-dot in the middletone region, and an inverted dispersed-dot (or negative image) in the shadow region. The nucleus randomization helps to minimize the distinctive texture in the highlight region, and the high frequency clustered-dot helps to reduce dot gain and put some regularity into the dot pattern to minimize the noisy appearance. This study has shown that the microcluster dots possess the high tone levels (enough to simulate the continuous tone appearance under normal viewing conditions) and high frequency screen characteristics. Granted that the larger the cell size the better for the stochastic screening, one does not need a very large supercell, like 256×256 array, to achieve good renditions. Smooth renditions can be achieved by using relatively small dots with a few hundred of tone levels. This study further supports the claims made in an early paper that[8]

1. it can apply to any digital halftone cells,
2. it provides both high frequency and high tone level screens,
3. it gives relatively smooth transition of gray levels,
4. it introduces irregularity to often rigid dispersed halftone patterns,
5. it adds many more angle-frequency-level combinations that are unattainable by the rational screens,
6. it provides a variety of ways for arranging the dot shape and dot pattern,
7. it uses threshold array approach; therefore, it can be implemented in a two-dimensional look up table using Holladay's algorithm which is the most efficient way of implementing halftone screens,
8. the memory requirement and computation cost are very low,
9. the processing speed is very fast, and
10. it can achieve a high precision for 15 and 75-degree screens.

References

1. H. R. Kang, Color Technology for Electronic Imaging Devices, pp: 230, SPIE Optical Engineering Press, Bellingham, Washington (1997).
2. J. P. Allebach and B. Liu, "Random quasi-periodic halftone process," J. Opt. Soc. Am., 66: 909-917 (1976).
3. J. P. Allebach, "Random nucleated halftone screening," Photogr. Sci. Eng., Vol. 22: 89-91 (1978).

4. R. A. Ulichney, "Dithering with blue noise," Proc. IEEE, Vol. 76: 56-79 (1988).
5. T. Mitsa and K. Parker, "Digital halftoning using a blue noise mask," Proc. SPIE 1452: 47-56 (1991).
6. K. Parker, T. Mitsa, and R. Ulichney, "A new algorithm for manipulating the power spectrum of halftone pattern," Proc. SPSE 7th Int'l Congress on Non-Impact Printing, pp. 471-475 (1991).
7. R. Ulichney, 'The void-and-cluster method for dither array generation," Proc. SPIE 1913: 332-343 (1993).
8. H. R. Kang, "Dispersed Micro-Cluster Halftoning," IS&T's 11th International Congress on Adv. In Non-Impact Printing Technologies, pp: 427-430 (1995).
9. P. Fink, PostScript screening: Adobe accurate screens, Chapter 4: 43-61, Adobe Press, Mountain View, CA (1992).
10. H. R. Kang, Color Technology for Electronic Imaging Devices, Chapter 9: 208-261, SPIE Optical Engineering Press, Bellingham, Washington (1997).
11. B. E. Bayer, "An optimum method for two-level rendition of continuous-tone pictures," IEEE International Conf. On Communication, Vol. 1: 26-11 to 26-15 (1973).
12. D. Kermisch and P. G. Roetling, "Fourier spectrum of halftone images," J. Opt. Soc. Am., Vol. 65: 716-723 (1975).
13. J. P. Allebach and B. Liu, "Analysis of halftone dot profile and aliasing in the discrete binary representation on images," J. Opt. Soc. Am., Vol. 67:1147-1154 (1977).
14. R. A. Ulichney, Digital Halftoning, The MIT Press, Cambridge (1987).
15. R. A. Ulichney, "Frequency analysis of ordered dither," SPIE Vol. 1079 Hard Copy Output: 361-373 (1989).
16. R. N. Brace, The Fourier Transform and Its Application, pp. 370, McGraw-Hill, New York (1978).
17. T. M. Holladay, "An optimum algorithm for halftone generation for displays and hard copies," Proc. SID, Vol. 21: 185-192 (1980).
18. A. R. Weeks, Jr., Fundamentals of Electronic Image Processing, SPIE/IEEE Series on Imaging Science & Engineering. P: 59 (1996).

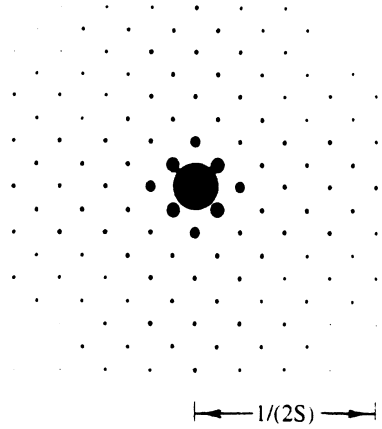

Fig. 10a. The clustered dot.

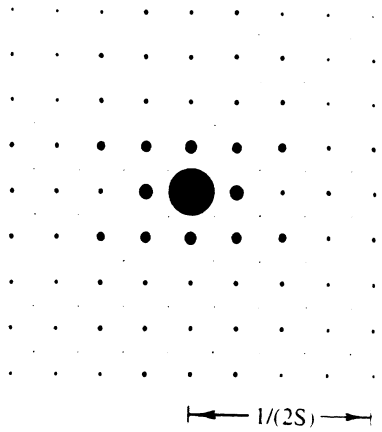

Fig. 10b. The dual-dot.

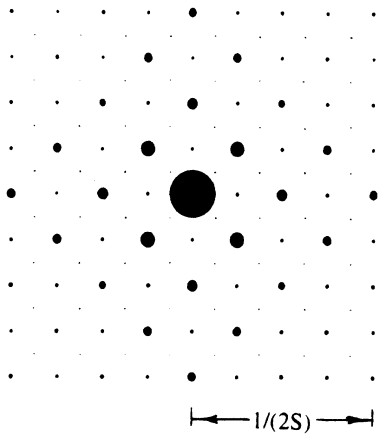

Fig. 10c. The quad-dot.

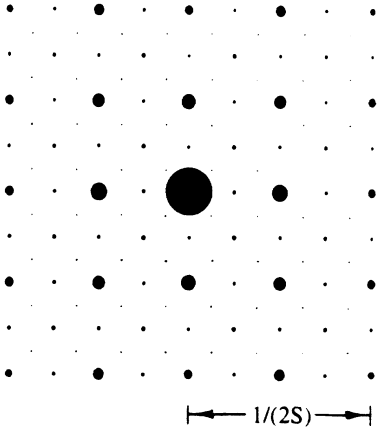

Fig. 10d. The Octa-dot.

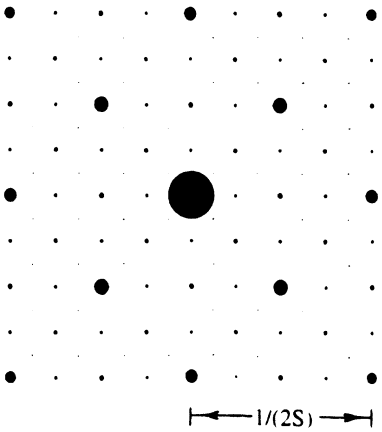

Fig. 10e. The hexdeca-dot.

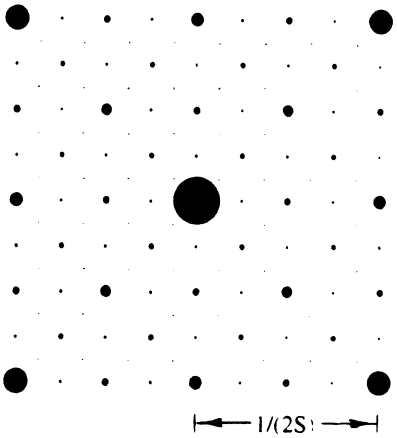

Fig. 10f. The dispersed-dot.

Figure 10. Fourier exposure plots of the 45-degree and 128 level screen with different subdivisions.

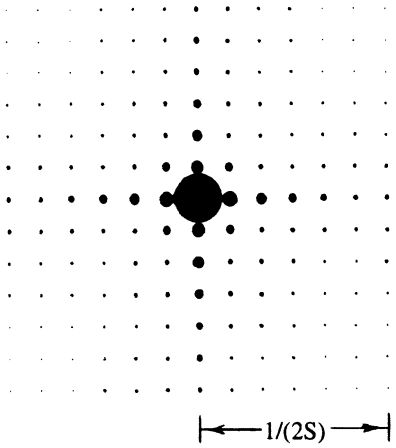

Fig. 11a. The clustered dot.

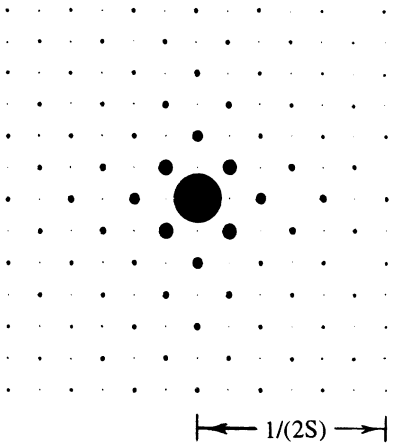

Fig. 11b. The dual-dot.

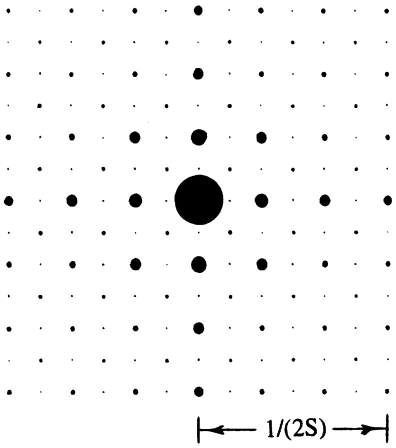

Fig. 11c. The quad-dot.

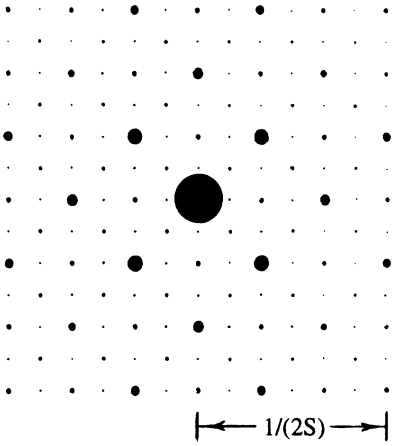

Fig. 11d. The octa-dot.

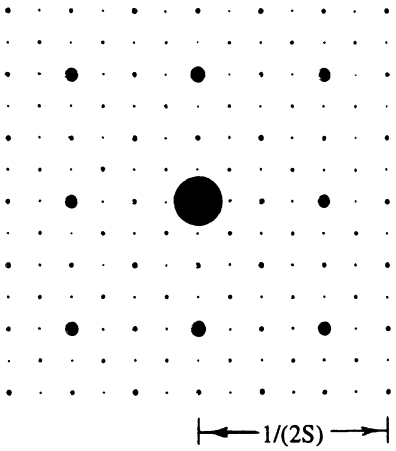

Fig. 11e. The hexceca-dot.

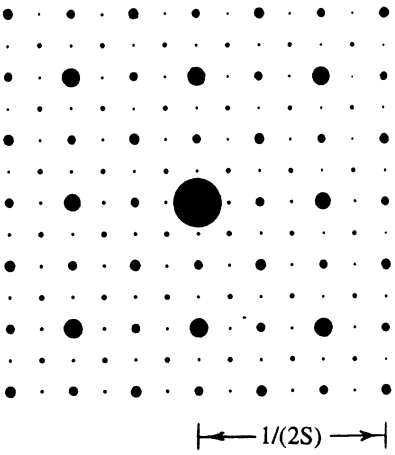

Fig. 11f. The dispersed-dot.

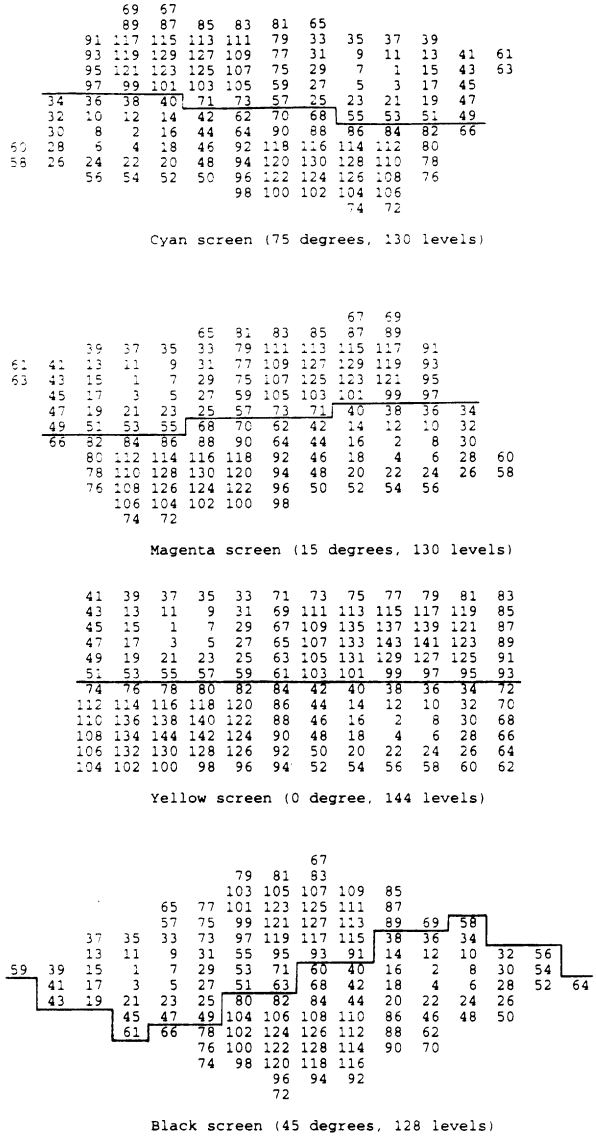

Figure 12. Threshold arrays of dual-dots

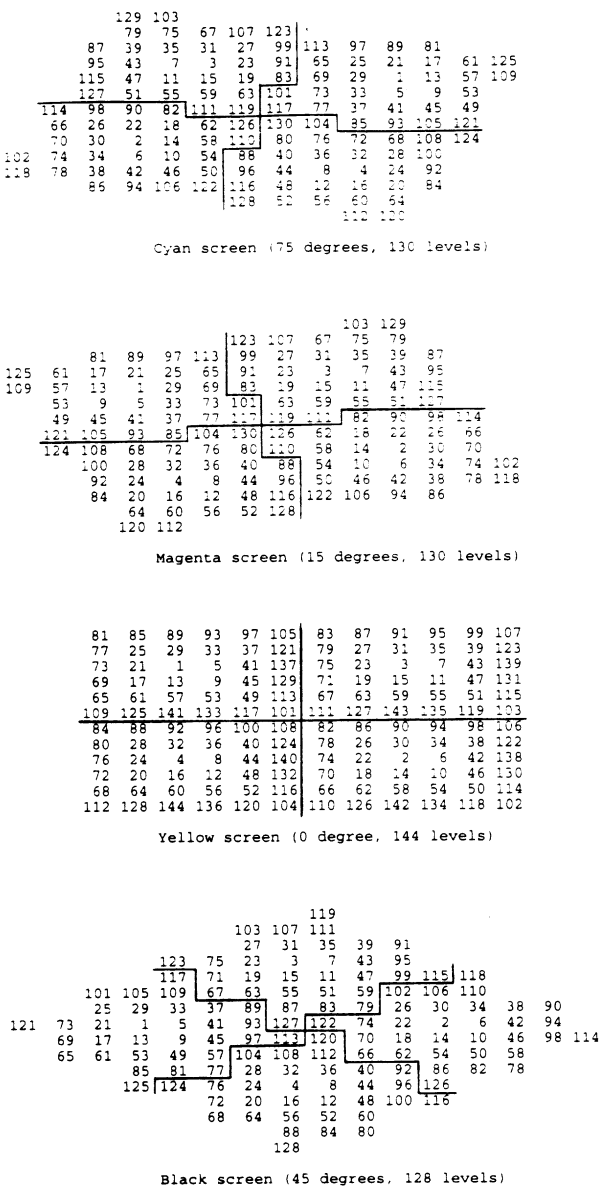

Figure 13. Threshold arrays of quad-dots.

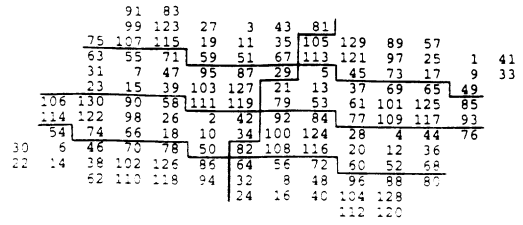

Cyan screen (75 degrees, 130 levels)

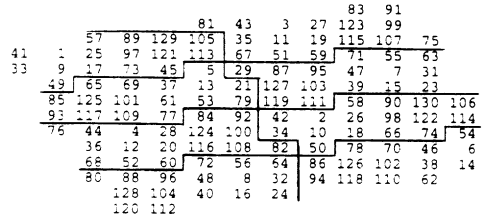

Magenta screen (15 degrees, 130 levels)

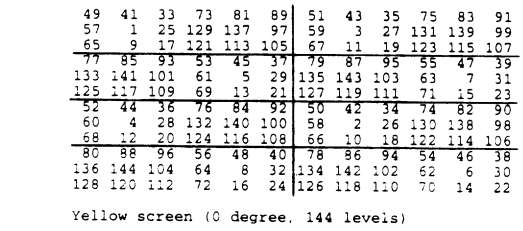

Yellow screen (0 degree, 144 levels)

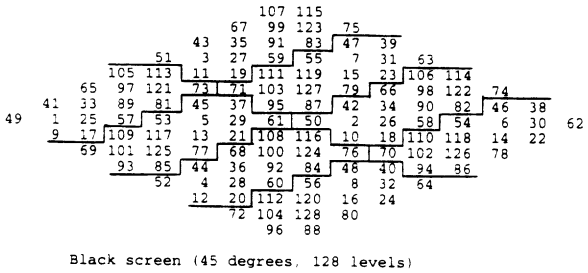

Black screen (45 degrees, 128 levels)

Figure 14. Threshold arrays of octa-dots

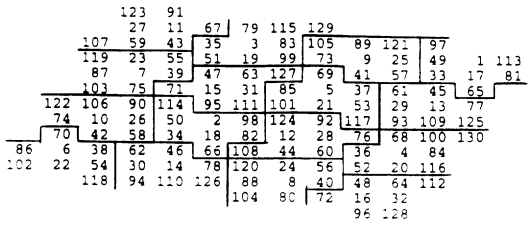

Cyan screen (75 degrees, 130 levels)

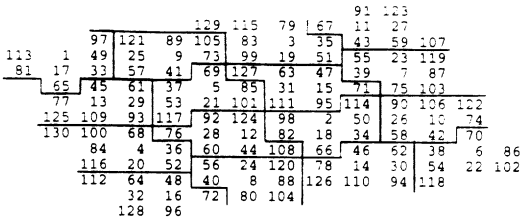

Magenta screen (15 degrees, 130 levels)

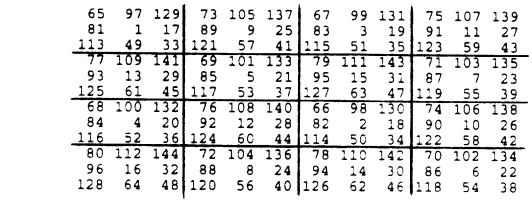

Yellow screen (0 degree, 144 levels)

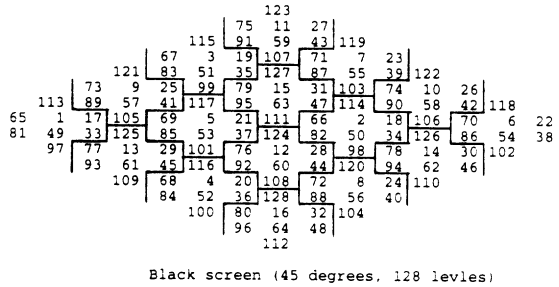

Black screen (45 degrees, 128 levles)

Figure 15. Threshold arrays of hexdeca-dots